Computer Methods in Applied Mechanics and Engineering 90 (1991) 829–844
North-Holland

2D finite elements with displacement interpolated embedded localization lines: The analysis of fracture in frictional materials

Eduardo N. Dvorkin
Center for Industrial Research, Fudetec, Buenos Aires, Argentina

Andrea P. Assanelli
Center for Industrial Research, Fudetec, Buenos Aires, Argentina

Received 30 August 1990
Revised manuscript received 7 February 1991

The finite element modelling of fracture problems in frictional materials is investigated. Displacement interpolated localization lines embedded in quadrilateral 2D elements based on mixed interpolation of tensorial components (QMITC) are used for the analyses.

1. Introduction

A reliable computational modelling of 2D fracture problems in frictional materials requires the following three ingredients:

(i) A finite element formulation that in the pre-fracture regime provides reliable results. That is to say, a finite element formulation that satisfies the following requirements:
- The elements do not contain spurious zero-energy modes.
- The elements satisfy Irons' Patch Test.
- The predictive capability of the elements is high and relatively insensitive to element distortions and changes in material properties (e.g. in the case of elasto-plastic problems the elements must not lock in the fully plastic range)

The quadrilateral 2D element QMITC developed in [1] satisfies the above requirements.

(ii) A fracture formulation to be used with the above elements. This formulation has to assure a correct fracture energy dissipation when the mesh is refined (objectivity with regard to regular mesh refinement) and a correct fracture energy dissipation when the mesh is distorted (objectivity with regard to mesh distortion).
The formulation of finite elements with displacement interpolated embedded localization lines developed in [2] satisfies the above requirements.

(iii) An adequate constitutive relation for the pre-failure and ductile post-failure regimes, e.g. the constitutive relation for concrete developed in [3].

In this paper we concentrate on the first two ingredients, that is to say, we investigate the

performance of displacement interpolated localization lines embedded in QMITC elements for the analysis of fracture in frictional materials.

2. The QMITC Element

In the present section we summarize the formulation of the QMITC element. A detailed description of this element was presented in [1].

The 2D quadrilateral element QMITC is based on the method of *mixed interpolation of tensorial components* [4–6], hence we adopt a displacement interpolation and a strain interpolation and tie both interpolations together.

To interpolate displacements we use the interpolation functions of a five node isoparametric element [7] (see Fig. 1(a)).

The strain tensor at any point inside the element can be written using covariant components and contravariant base vectors,

$$\underline{\underline{\boldsymbol{\varepsilon}}} = \hat{\varepsilon}_{ij}\hat{\boldsymbol{g}}^i\hat{\boldsymbol{g}}^j \,. \tag{1}$$

In the natural coordinate system of an element, the covariant base vectors ($\boldsymbol{g}_i$) and the contravariant base vectors ($\boldsymbol{g}^i$) are defined as usual, and we use

$$\hat{\boldsymbol{g}}_i = \boldsymbol{g}_i|_{r=s=O} \,, \quad i=1,2,3 \,, \qquad \hat{\boldsymbol{g}}^i = \boldsymbol{g}^i|_{r=s=O} \,, \quad i=1,2,3 \,. \tag{2}$$

To interpolate the strain field inside the element we use the following interpolation functions:

$$\hat{\varepsilon}_{rr} = \hat{\varepsilon}_{rr}|_O^{\mathrm{DI}} + \frac{\sqrt{3}}{2}\left(\hat{\varepsilon}_{rr}|_D^{\mathrm{DI}} - \hat{\varepsilon}_{rr}|_B^{\mathrm{DI}}\right)\frac{|J_O|}{|J|}\,r + \frac{\sqrt{3}}{2}\left(\hat{\varepsilon}_{rr}|_A^{\mathrm{DI}} - \hat{\varepsilon}_{rr}|_C^{\mathrm{DI}}\right)\frac{|J_O|}{|J|}\,s \,, \tag{3a}$$

$$\hat{\varepsilon}_{ss} = \hat{\varepsilon}_{ss}|_O^{\mathrm{DI}} + \frac{\sqrt{3}}{2}\left(\hat{\varepsilon}_{ss}|_D^{\mathrm{DI}} - \hat{\varepsilon}_{ss}|_B^{\mathrm{DI}}\right)\frac{|J_O|}{|J|}\,r + \frac{\sqrt{3}}{2}\left(\hat{\varepsilon}_{ss}|_A^{\mathrm{DI}} - \hat{\varepsilon}_{ss}|_C^{\mathrm{DI}}\right)\frac{|J_O|}{|J|}\,s \,, \tag{3b}$$

$$\hat{\varepsilon}_{rs} = \hat{\varepsilon}_{rs}|_O^{\mathrm{DI}} \,. \tag{3c}$$

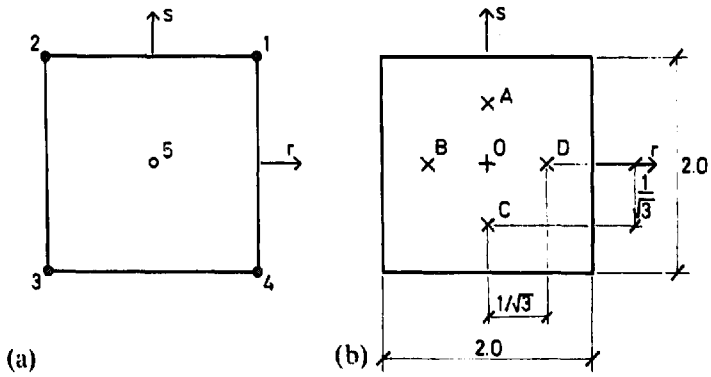

Fig. 1. Interpolations used in the QMITC element. (a) Displacement interpolation nodes. (b) Strain interpolation sample points.

For axisymmetric analysis, we interpolate the hoop strain using [8]

$$\hat{\varepsilon}_{tt} = \hat{\varepsilon}_{tt}|_O^{\mathrm{DI}} + \frac{\sqrt{3}}{2}(\hat{\varepsilon}_{tt}|_D^{\mathrm{DI}} - \hat{\varepsilon}_{tt}|_B^{\mathrm{DI}})\frac{|J_O|}{|J|}r + \frac{\sqrt{3}}{2}(\hat{\varepsilon}_{tt}|_A^{\mathrm{DI}} - \hat{\varepsilon}_{tt}|_C^{\mathrm{DI}})\frac{|J_O|}{|J|}s\,. \tag{3d}$$

In (3) we use the following notation:
- $\hat{\varepsilon}_{ij}|^{\mathrm{DI}}_{A,B,C,D,O}$ are the covariant strain components at points A, B, C, D and O (see Fig. 1(b)) directly evaluated from the displacement interpolation.
- $|J_0|$ is the determinant of the Jacobian at the element center.
- $|J|$ is the determinant of the Jacobian at a point of natural coordinates (r, s).

The two displacements corresponding to node 5 in Fig. 1(a) are condensed at the element level (see [1, Appendix II]).

In [1] it was shown that the QMITC element presents the following distinct features:
- It does not contain spurious zero-energy modes.
- It satisfies Irons' Patch Test.
- One rectangular element can exactly model a state of constant bending in plane stress.
- The predictive capability of the element is quite insensitive to element distortions.

In [9] it was shown that the QMITC element provides accurate results in the fully plastic range (non-locking behavior) and it can therefore be used for the calculation of plastic limit loads.

The stiffness matrix of the QMITC element is calculated using 2×2 Gauss numerical integration.

3. Finite elements with displacement interpolated embedded localization lines

3.1. Basic concepts

It has been shown in the literature [10–15] that for modelling strain-softening situations (e.g. the behaviour of concrete when fracture develops) in order to obtain objective results with regard to regular mesh refinement, the *fracture energy* has to be used as a material property to develop the stress-average strain constitutive relations.

Following the above consideration, two main development routes, which are closely related [16], have been proposed for the modelling of fracture problems in frictional materials:
- the smeared crack approach [12, 13, 17],
- the discrete crack approach [11].

However other formulations aimed at modelling strain localization problems have been proposed and some of them are discussed in [2].

In [2] a new formulation was developed for modelling strain localization problems, this new formulation fulfils the following requirements:
- Retains the desirable features of the smeared crack approach, namely the ability to model the progression of strain localization zones without remeshing and, for fracture problems, the use of an energy criterion in order to obtain results objective with regard to regular mesh refinement.
- Achieves the additional capability of being objective with regard to mesh distortions, thus

assuring a correct energy dissipation in fracture problems even when distorted meshes are used.

The main aspects in this new formulation are

- The strain localization involves a complete element as the minimum information quantum [18–20], instead of working at the integration points level as is usual in most of the available techniques.
- The strain localization (fracture) inside an element is considered in the form of a displacement discontinuity line embedded in the element domain.
- Once a localization line has been triggered in an element, two different constitutive relations are considered. First, a stress–displacement law for the discontinuity line, in the present case of fracture problems this law must be adjusted to the fracture energy value. Second, a conventional stress–strain law (hiperelasticity or hipoelasticity) for the element domain (see e.g. [3] for the case of concrete).
- The resulting finite elements are nonconforming. Hence for a reliable analysis capability, the elements with the displacement interpolated embedded localization line must not contain zero-energy modes and must satisfy an ad hoc version of Irons' Patch Test.

As shown in [2], these requirements are satisfied by the proposed formulation.

3.2. *The new formulation*

In this section we summarize the formulation of finite elements with displacement interpolated localization lines. A detailed description of this formulation was presented in [2].

We assume the solid shown in Fig. 2 in equilibrium at time (load level) t. At this time the localization (fracture) phenomenon has already been triggered and is modelled as a displacement discontinuity line. We seek the equilibrium configuration at time (load level) $t+\Delta t$. At this configuration the Principle of Virtual Work must be satisfied. Assuming a material nonlinear only analysis and using Bathe's notation [2, 7],

$$\int_{V_1} \delta \boldsymbol{e}^{\mathrm{t}\ t+\Delta t}\boldsymbol{\sigma}\, \mathrm{d}V_1 + \int_{V_2} \delta \boldsymbol{e}^{\mathrm{t}\ t+\Delta t}\boldsymbol{\sigma}\, \mathrm{d}V_2 = \int_{S_1} \delta \boldsymbol{u}^{\mathrm{t}\ t+\Delta t}\boldsymbol{p}_1\, \mathrm{d}S_1 + \int_{S_2} \delta \boldsymbol{u}^{\mathrm{t}\ t+\Delta t}\boldsymbol{p}_2\, \mathrm{d}S_2 + \int_{A_1} \delta \boldsymbol{u}^{\mathrm{t}\ t+\Delta t}\boldsymbol{r}_1\, \mathrm{d}A_1 + \int_{A_2} \delta \boldsymbol{u}^{\mathrm{t}\ t+\Delta t}\boldsymbol{r}_2\, \mathrm{d}A_2 . \quad (4)$$

In (4) $\boldsymbol{e}$ is the vector containing the Cartesian components of the incremental infinitesimal strain tensor, ${}^{t+\Delta t}\boldsymbol{\sigma}$ is the vector containing the Cartesian components of the Cauchy stress tensor at time $t+\Delta t$, and $\boldsymbol{u}$ is the vector containing the Cartesian components of the incremental displacements.

For the other terms in (4), Fig. 2 is self-explanatory.

We now introduce the finite element discretization. Prior to localization and when using the QMITC element, the incremental displacement and strain interpolations are the ones commented in Section 2.

After localization is triggered based on a given criterion (see Section 3.3.1), and therefore a displacement discontinuity line is opened in a QMITC element (see Fig. 3), we introduce the vector $\hat{\boldsymbol{U}}^{c}$ containing the components, in a local Cartesian system $(\hat{x}_1, \hat{x}_2)$, of the rigid

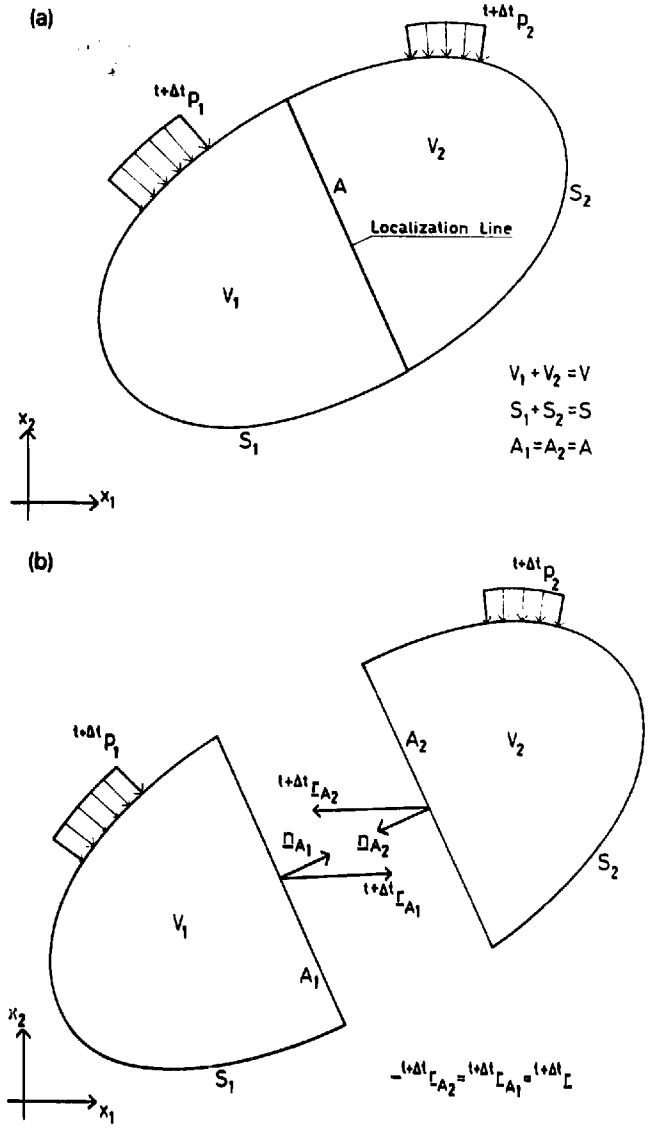

Fig. 2. Solid with a localization line. (a) solid, (b) split solid.

incremental displacement that takes V_2 away from V_1 (Fig. 3):

$$\hat{\boldsymbol{U}}^c = \begin{bmatrix} \hat{v}^c \\ \hat{w}^c \end{bmatrix}. \tag{5}$$

Being $\boldsymbol{R}$ the matrix that rotates Cartesian vector components from the $(\hat{x}_1, \hat{x}_2)$ system to the global Cartesian system, the resulting displacement interpolations for the left subdomain V_1 and for the right subdomain V_2 are

$$\boldsymbol{u}_1 = \boldsymbol{H}(\boldsymbol{U} - \boldsymbol{\phi}\boldsymbol{R}\hat{\boldsymbol{U}}^c), \qquad \boldsymbol{u}_2 = \boldsymbol{H}(\boldsymbol{U} - \boldsymbol{\phi}\boldsymbol{R}\hat{\boldsymbol{U}}^c) + \boldsymbol{R}\hat{\boldsymbol{U}}^c, \tag{6}$$

where $\boldsymbol{U}$ is the incremental nodal displacements vector.

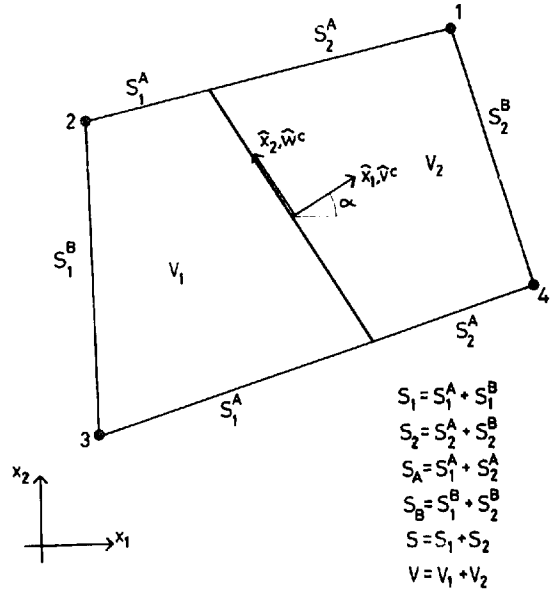

Fig. 3. QMITC element with an embedded localization line.

In the above $\boldsymbol{H}$ is the standard interpolation matrix for a 5-node isoparametric element [7] and $\boldsymbol{\phi}$ is defined as

$$\boldsymbol{\phi} = [\boldsymbol{\phi}_1 \quad \boldsymbol{\phi}_2 \quad \boldsymbol{\phi}_3 \quad \boldsymbol{\phi}_4]^t . \tag{7}$$

Each of the submatrices $\boldsymbol{\phi}_i$ of dimension 2×2 depends on the position of node i relative to the localization line, according to the following rule:

$$\boldsymbol{\phi}_i = \begin{cases} \mathbf{0} & \text{when node } i \in V_1 , \\ \mathbf{I} & \text{when node } i \in V_2 . \end{cases}$$

A computational problem appears when within round-off tolerances a localization line passes through a node and the definition of $\boldsymbol{\phi}_i$ is ambiguous. For this case, in our implementation we adopted the arbitrary criterion of using for the α angle in Fig. 3 a value of $\alpha + \Delta\alpha$ where $\Delta\alpha << \alpha$ and is of arbitrary sign.

For two neighbour points, one on the right and one on the left of the localization line, the incremental displacement discontinuity is given by

$$\boldsymbol{u}^+ - \boldsymbol{u}^- = \boldsymbol{R}\hat{\boldsymbol{U}}^c . \tag{8}$$

Using the strain interpolation of (3), a strain–displacement matrix $\hat{\boldsymbol{B}}$ is obtained, hence for any element point either on V_1 or on V_2,

$$\boldsymbol{e} = \hat{\boldsymbol{B}}(\boldsymbol{U} - \boldsymbol{\phi}\boldsymbol{R}\hat{\boldsymbol{U}}^c) = \hat{\boldsymbol{B}}\boldsymbol{U}^{EP} . \tag{9}$$

Replacing in (4), and taking into account that $\delta\boldsymbol{U}$ and $\delta\hat{\boldsymbol{U}}^c$ are independent variations we

obtain the following two sets of equations (details of the derivation for a general element are given in [2]):

$$\int_V \hat{\boldsymbol{B}}^{t\,t+\Delta t}\boldsymbol{\sigma}\,\mathrm{d}V = \int_S \boldsymbol{H}_s^{t\,t+\Delta t}\boldsymbol{p}\,\mathrm{d}S\,, \tag{10a}$$

$$\boldsymbol{R}^t\boldsymbol{\phi}^t \int_V \hat{\boldsymbol{B}}^{t\,t+\Delta t}\boldsymbol{\sigma}\,\mathrm{d}V = \boldsymbol{R}^t\boldsymbol{\phi}^t \int_{S^A} H_{S^A}^{t\,t+\Delta t}\boldsymbol{p}\,\mathrm{d}S^A - \int_{S_2^A} \boldsymbol{R}^{t\,t+\Delta t}\boldsymbol{p}_2\,\mathrm{d}S_2^A + \int_A^{t+\Delta t\,t+\Delta t}\hat{\boldsymbol{r}}\,\mathrm{d}A\,. \tag{10b}$$

Equation (10a) is the standard set of global equilibrium equations.

In [2], (10b) was worked out together with the *additional condition* of global equilibrium for each of the two parts into which the localization line subdivides the element, i.e.,

$$\int_{S_2} \boldsymbol{R}^{t\,t+\Delta t}\boldsymbol{p}_2\,\mathrm{d}S_2 = \int_A {}^{t+\Delta t}\underline{\underline{\boldsymbol{\sigma}}} \circ \boldsymbol{n}_A\,\mathrm{d}A\,, \tag{11}$$

where ${}^{t+\Delta t}\underline{\underline{\boldsymbol{\sigma}}}$ is a second order tensor, $\boldsymbol{n}^A$ is a unit vector normal to the localization line and the dot indicates a scalar product.

By properly defining a matrix $\boldsymbol{\psi}$ we can write

$${}^{t+\Delta t}\underline{\underline{\boldsymbol{\sigma}}} \circ \boldsymbol{n}_A = \boldsymbol{\psi}\,{}^{t+\Delta t}\boldsymbol{\sigma}\,. \tag{12}$$

After some algebra and using (11) and (12), (10b) can be stated as

$$\int_A \boldsymbol{\psi}\,{}^{t+\Delta t}\boldsymbol{\sigma}\,\mathrm{d}A = \int_A {}^{t+\Delta t}\hat{\boldsymbol{r}}\,\mathrm{d}A\,. \tag{13}$$

Considering that

$${}^{t+\Delta t}\boldsymbol{\sigma} = {}^t\boldsymbol{\sigma} + {}_t\boldsymbol{\sigma}\,, \qquad {}^{t+\Delta t}\hat{\boldsymbol{r}} = {}^t\hat{\boldsymbol{r}} + {}_t\hat{\boldsymbol{r}} \tag{14}$$

and that the configuration at t fulfils equilibrium, (13) can be written in incremental form as

$$\int_A \boldsymbol{\psi}\,{}_t\boldsymbol{\sigma}\,\mathrm{d}A = \int_A {}_t\hat{\boldsymbol{r}}\,\mathrm{d}A\,. \tag{15}$$

We now introduce the following constitutive relations:

– For the material on both sides of the localization line,

$${}^{t+\Delta t}\boldsymbol{\sigma} = {}^t\boldsymbol{\sigma} + \int_e {}_tC\,\mathrm{d}\boldsymbol{e}\,, \tag{16a}$$

where ${}_tC$ is the tangent constitutive matrix corresponding to a general material without fracture considerations (e.g. the elastoplastic material model developed in [3] for concrete).

– For the localization line,

$${}^{t+\Delta t}\hat{\boldsymbol{r}} = {}^t\hat{\boldsymbol{r}} + \int_{\hat{U}^c} {}_t\hat{C}^c\,\mathrm{d}\hat{U}^c\,. \tag{16b}$$

As we stated above, in fracture problems the definition of (16b) has to assure a correct fracture energy dissipation (see Section 3.3.3).

For the *linearized step*,

$$\left[\int_V \hat{\boldsymbol{B}}^{\mathrm{t}}\, {}_{t}\boldsymbol{C}\hat{\boldsymbol{B}}\, \mathrm{d}V\right](\boldsymbol{U} - \boldsymbol{\phi}\boldsymbol{R}\hat{\boldsymbol{U}}^{\mathrm{c}}) = {}^{t+\Delta t}\boldsymbol{P} - {}^{t}\boldsymbol{F}\,, \tag{17a}$$

$$\hat{\boldsymbol{U}}^{\mathrm{c}} = \boldsymbol{S}_{cc}^{-1}\boldsymbol{S}_{UU}\boldsymbol{U}\,. \tag{17b}$$

In the above,

$${}^{t+\Delta t}\boldsymbol{P} = \int_S \boldsymbol{H}_S^{\mathrm{t}}\, {}^{t+\Delta t}\boldsymbol{p}\, \mathrm{d}S\,, \qquad {}^{t}\boldsymbol{F} = \int_V \hat{\boldsymbol{B}}^{\mathrm{t}}\, {}^{t}\boldsymbol{\sigma}\, \mathrm{d}V\,, \tag{18a,b}$$

$$\hat{\boldsymbol{S}}_{cc} = \int_A (\boldsymbol{\psi}\, {}_{t}\boldsymbol{C}\hat{\boldsymbol{B}}\boldsymbol{\phi}\boldsymbol{R} + {}_{t}\hat{\boldsymbol{C}}^{\mathrm{c}})\, \mathrm{d}A\,, \qquad \boldsymbol{S}_{UU} = \int_A \boldsymbol{\psi}\, {}_{t}\boldsymbol{C}\hat{\boldsymbol{B}}\, \mathrm{d}A\,. \tag{18c,d}$$

Replacing with (17b) in (17a) we obtain

$$\left[\int_V \hat{\boldsymbol{B}}^{\mathrm{t}}\, {}_{t}\boldsymbol{C}\hat{\boldsymbol{B}}(\mathbf{I} - \boldsymbol{\phi}\boldsymbol{R}\boldsymbol{S}_{CC}^{-1}\boldsymbol{S}_{UU})\, \mathrm{d}V\right]\boldsymbol{U} = {}^{t+\Delta t}\boldsymbol{P} - {}^{t}\boldsymbol{F}\,. \tag{19}$$

The term between brackets on the left-hand side of (19) is the non-symmetric consistent tangent stiffness matrix. In [2] the computational efficiencies of several symmetric even though non-consistent stiffness matrices (${}^{\tau}\boldsymbol{K}$) were discussed.

The final equilibrium configuration at $t + \Delta t$ is obtained iterating
- at the element level on (15)
- at the model assembly level, when using load control [7], on the following equations for the i-th iteration:

$${}^{\tau}\boldsymbol{K}\,\Delta\boldsymbol{U}^{(i)} = {}^{t+\Delta t}\boldsymbol{P} - {}^{t+\Delta t}\boldsymbol{F}^{(i-1)}\,, \tag{20a}$$

$$\boldsymbol{U}^{(i)} = \boldsymbol{U}^{(i-1)} + \Delta\boldsymbol{U}^{(i)}\,, \qquad \boldsymbol{U}^{(0)} = \mathbf{0}\,. \tag{20b,c}$$

The equilibrium configuration is obtained when a given convergence criterion is fulfilled (see [7, Chapter 8]).

For iterating in the load–displacement space, the iteration equations are given in [21].

3.3. *Computational details*

In our computational implementation the following details are relevant:

3.3.1. The Mode I fracture initiation criterion used for frictional materials (e.g. concrete) is shown in Fig. 4 and is discussed in [3]. When within an element the stress state is not constant, several ways of implementing the initiation criterion can be considered, e.g. the localization line can be opened either when at only one Gauss point the stress level reaches the failure surface or when the stress level at the element center reaches the failure surface or when the

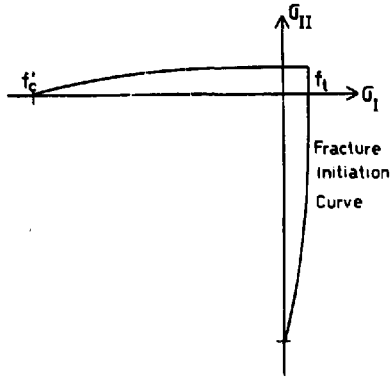

Fig. 4. Fracture initiation criterion.

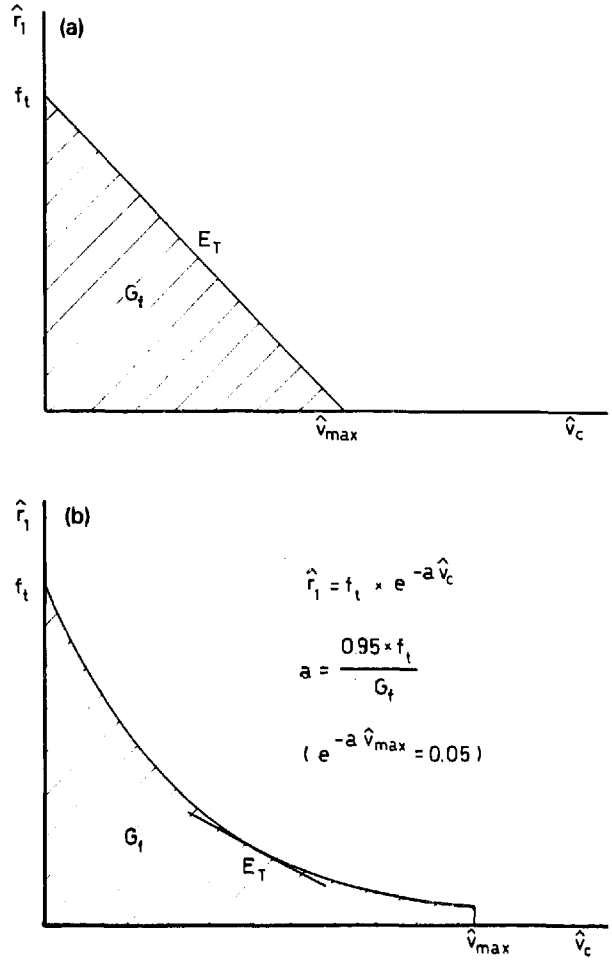

Fig. 5. Constitutive relation for the localization line. (a) Linear model, (b) exponential model.

stress levels at the four Gauss points reach the failure surface, etc. The third criterion is used in our implementation.

3.3.2. Non-orthogonal cracks (localization lines) can be opened in an element [15, 22, 23].

3.3.3. For the localization lines a stress–displacement incremental constitutive relation corresponding to Mode I blunt fracture is used:

$$\begin{bmatrix} {}_t\hat{r}_1 \\ {}_t\hat{r}_2 \end{bmatrix} = \begin{bmatrix} {}_tE_T({}^t\hat{v}_c) & 0 \\ 0 & {}_tG_T \end{bmatrix} \begin{bmatrix} \hat{v}_c \\ \hat{w}_c \end{bmatrix}, \tag{21}$$

where ${}_tE_T({}^t\hat{v}_c)$ is adjusted to a given fracture energy G_f (material property) and can be considered either a linear function or an exponential function (Fig. 5). In (21) ${}_tG_T$ is related to the instantaneous shear modulus via the well known 'shear retention factor' [3].

3.3.4. When a localization line has been opened inside an element, for the i-th iteration in (20), the following calculations are performed at the element level:

(i) $k=0$; ${}^{t+\Delta t}\hat{\boldsymbol{U}}^{c(i)}_{(0)} = {}^{t}\hat{\boldsymbol{U}}^{c}$

(ii) ${}^{t+\Delta t}\boldsymbol{U}^{EP(i)}_{(k)} = {}^{t+\Delta t}\boldsymbol{U}^{(i)} - {}^{t+\Delta t}\hat{\boldsymbol{U}}^{c(i)}_{(k)}$.

(iii) Calculate the incremental displacement of the interior (condensed) node, solving the following equation:

$$\begin{bmatrix} {}^{\tau}\boldsymbol{K}^{EP(i)}_{ee} & {}^{\tau}\boldsymbol{K}^{EP(i)}_{ei} \\ {}^{\tau}\boldsymbol{K}^{EP(i)}_{ie} & {}^{\tau}\boldsymbol{K}^{EP(i)}_{ii} \end{bmatrix} \begin{bmatrix} \Delta\boldsymbol{U}^{EP(i)}_{e(k)} \\ \Delta\boldsymbol{U}^{EP(i)}_{i(k)} \end{bmatrix} = \begin{bmatrix} {}^{t+\Delta t}\boldsymbol{P} \\ \boldsymbol{0} \end{bmatrix} - \begin{bmatrix} {}^{t+\Delta t}\boldsymbol{F}^{(i-1)}_{e} \\ {}^{t+\Delta t}\boldsymbol{F}^{(i-1)}_{i} \end{bmatrix}$$

(see [1, Appendix II]), the subindex 'i' refers to the interior (fifth) node and the subindex 'e' to the four exterior nodes and ${}^{\tau}\boldsymbol{K}^{EP}$ is given by the integral between brackets on the left-hand side of (17a).

(iv) Calculate the element incremental stresses using (9) and (16a) $({}_{t}\sigma^{(i)}_{(k)})$ (For the integration of the stress/strain relation details are given in [3]).

(v) Calculate the localization line incremental stresses using (16b) $({}_{t}\hat{r}^{(i)}_{(k)})$.

(vi) $$\Delta\hat{\boldsymbol{U}}^{c(i)}_{(k)} = \boldsymbol{S}^{-1}_{cc}\left[\int_A \boldsymbol{\psi}\, {}_{t}\boldsymbol{\sigma}^{(i)}_{(k)}\, dA - \int_A {}_{t}\hat{\boldsymbol{r}}^{(i)}_{(k)}\, dA\right].$$

(vii) If $(|\Delta\boldsymbol{U}^{c}|) < \text{TOL}$ then convergence at the element level has been achieved, if not

- ${}^{t+\Delta t}\hat{\boldsymbol{U}}^{c(i)}_{(k+1)} = {}^{t+\Delta t}\hat{\boldsymbol{U}}^{c(i)}_{(k)} + \Delta\hat{\boldsymbol{U}}^{c(i)}_{(k)}$
- $k = k+1$
- Go to (ii).

3.3.5. For elements where a localization line has been opened, the stress output is only relevant at the element center.

4. Numerical examples

In [1] and [9] the numerical experimentation showed that the QMITC element
(1) converges, that is to say that it is stable and consistent;
(2) provides efficient and accurate solutions for some linear and nonlinear benchmark problems.

In [2] the numerical experimentation showed that the formulation of displacement interpolated embedded localization lines for problems involving fracturing of frictional materials
(1) provides objective results with regard to regular mesh refinement;
(2) provides objective results with regard to mesh distortions in constant stress problems.

That is to say, in these problems the work of the external loads is correctly transformed into strain and fracture energy which is the physical idea behind Irons' Patch Test ([24, Chapter 2]). Hence we can confirm, since our formulation does not present zero energy modes, that the new formulation is stable and consistent.

Since our purpose in the present paper is to investigate the ability of the formulation to describe the fracture of frictional materials and we are not concerned with the accuracy of our model in the pre-failure and ductile post-failure regimes [3]. we use a simple elastic-fracture constitutive model for our numerical examples.

All the examples have been analyzed using the elastic stiffness matrix (symmetric) with a BFGS matrix updating technique [7]. In [2] this procedure was shown to be slightly less efficient than the procedure based on the symmetric part of the consistent stiffness matrix and a full Newton–Raphson iterative scheme, however the adopted iterative method seems to be more robust.

4.1. *Bending of a simply supported beam*

In Fig. 6 we show the results obtained using in undistorted and distorted meshes:
- standard 4N elements (STD-4N) + embedded localization lines,
- QMITC elements + embedded localization lines.

From the plotted load–displacement curves that correspond to a linear softening it is clear that
- the results deterioration due to mesh distortion is higher when using STD-4N elements than when using QMITC elements.
- the STD-4N elements produce results that are too stiff.

This problem was also examined in [2] and the conclusion there was that in order to achieve

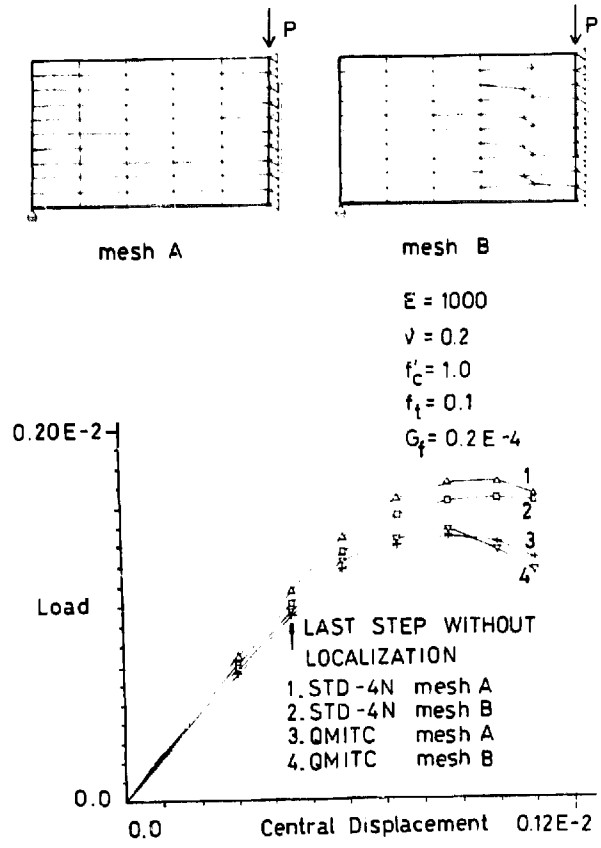

Fig. 6. Bending of plane stress simply supported beam.

objectivity with regard to mesh distortions, it is necessary to use the formulation of displacement interpolated embedded localization lines coupled to an element that is also quite insensitive to mesh distortions: the QMITC element.

4.2. Notched beam

The problem shown in Fig. 7 was analyzed in [25] using the discrete crack approach and in [15] using the smeared crack approach.

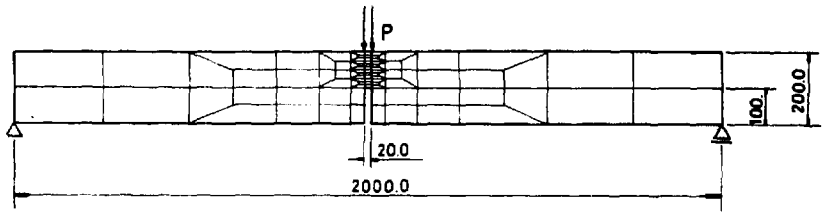

$E = 30000\ N/mm^2$
$\nu = 0.2$
$f'_c = 37\ N/mm^2$
$f_t = 3.33\ N/mm^2$
$G_f = 0.124\ N/mm$

Fig. 7a. Notched beam. Model.

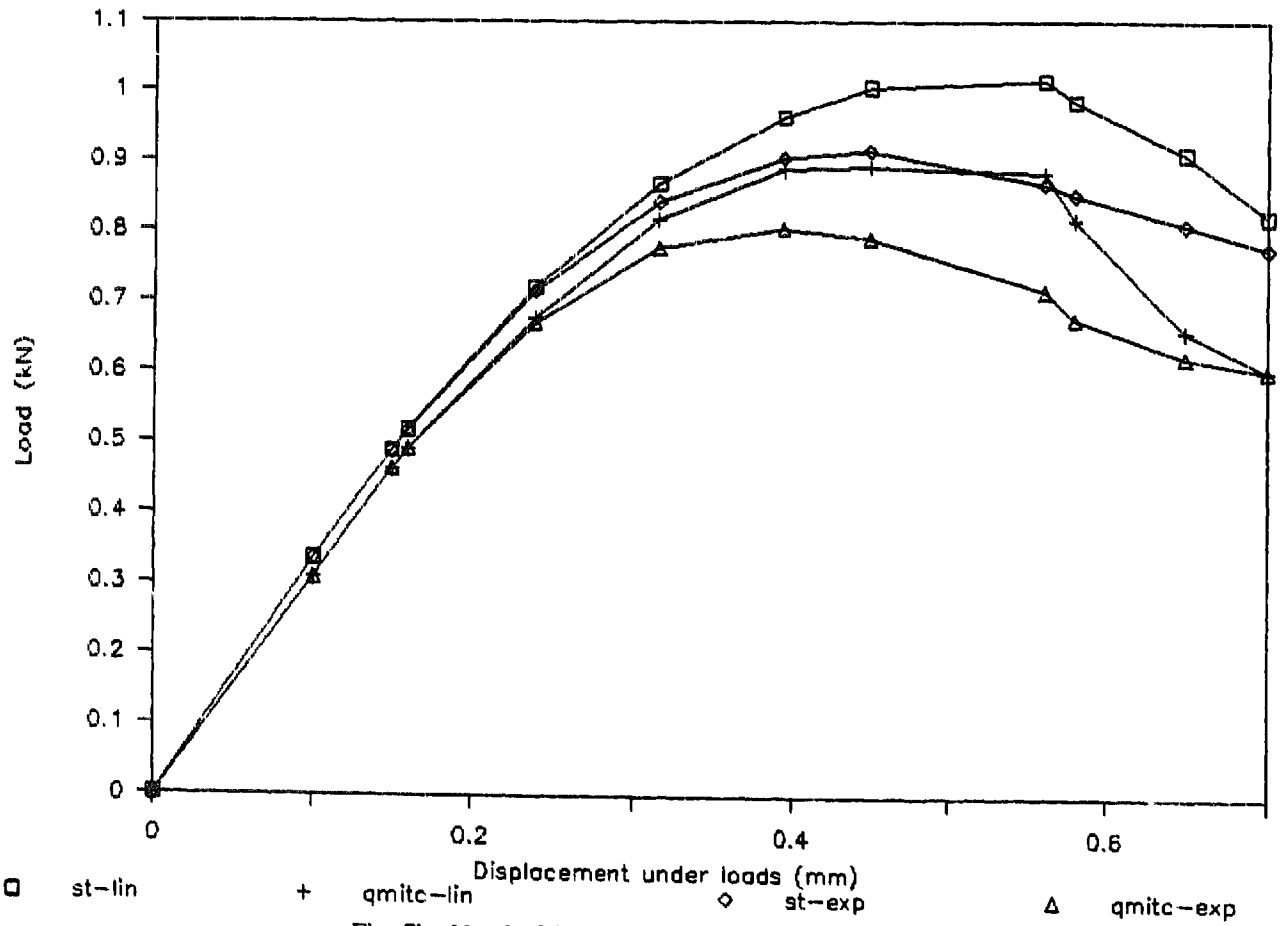

Fig. 7b. Notched beam. Load–displacement curves.

In Fig. 7 we show the results we obtained for linear and exponential softening using
- STD-4N elements + embedded localization lines,
- QMITC elements + embedded localization lines.

It is apparent once again that the STD-4N elements produce results that are too stiff.

4.3. *Deep beam under two point loading*

The experimental testing of this problem was reported in [26] and the conclusions were
- the beam failed by a diagonal tension mode (the fracture plane is indicated with a dotted line in Fig. 8);
- there was no significant fall in the load at the time of formation of the diagonal crack;
- there was no crushing of the compression zone.

In Fig. 8 we show the load–deflection curve and the fracture patterns for different load levels that we obtained with cur analysis technique using an exponential softening. The finite element results present a close agreement with the experimental observations. For this case a realistic finite element solution was also reported in [27].

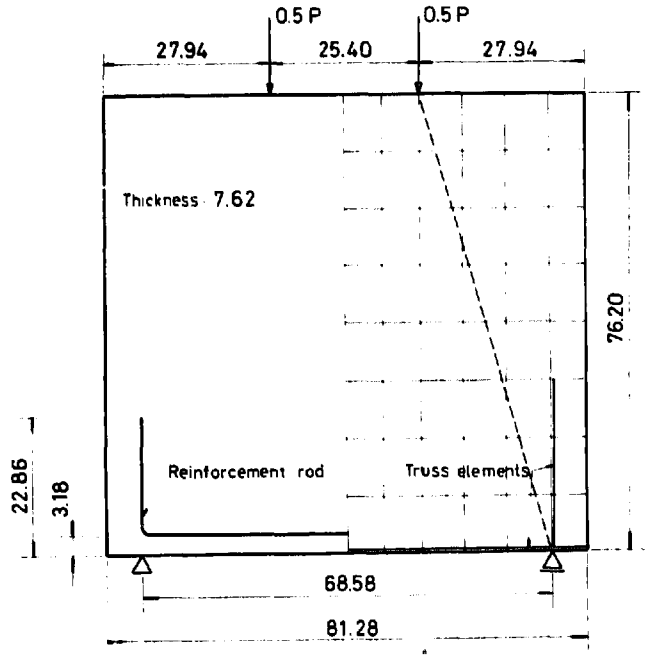

Concrete: $E = 230000$ kg/cm^2
$\nu = 0.2$
$f'_c = 278$ kg/cm^2
$f_t = 17.5$ kg/cm^2
$G_f = 0.075$ kg/cm

Steel rod: $A = 0.713$ cm^2
$E = 2100000$ kg/cm^2
$\sigma_y = 3200$ kg/cm^2

Fig. 8(a). Deep beam under two point loading. Model.

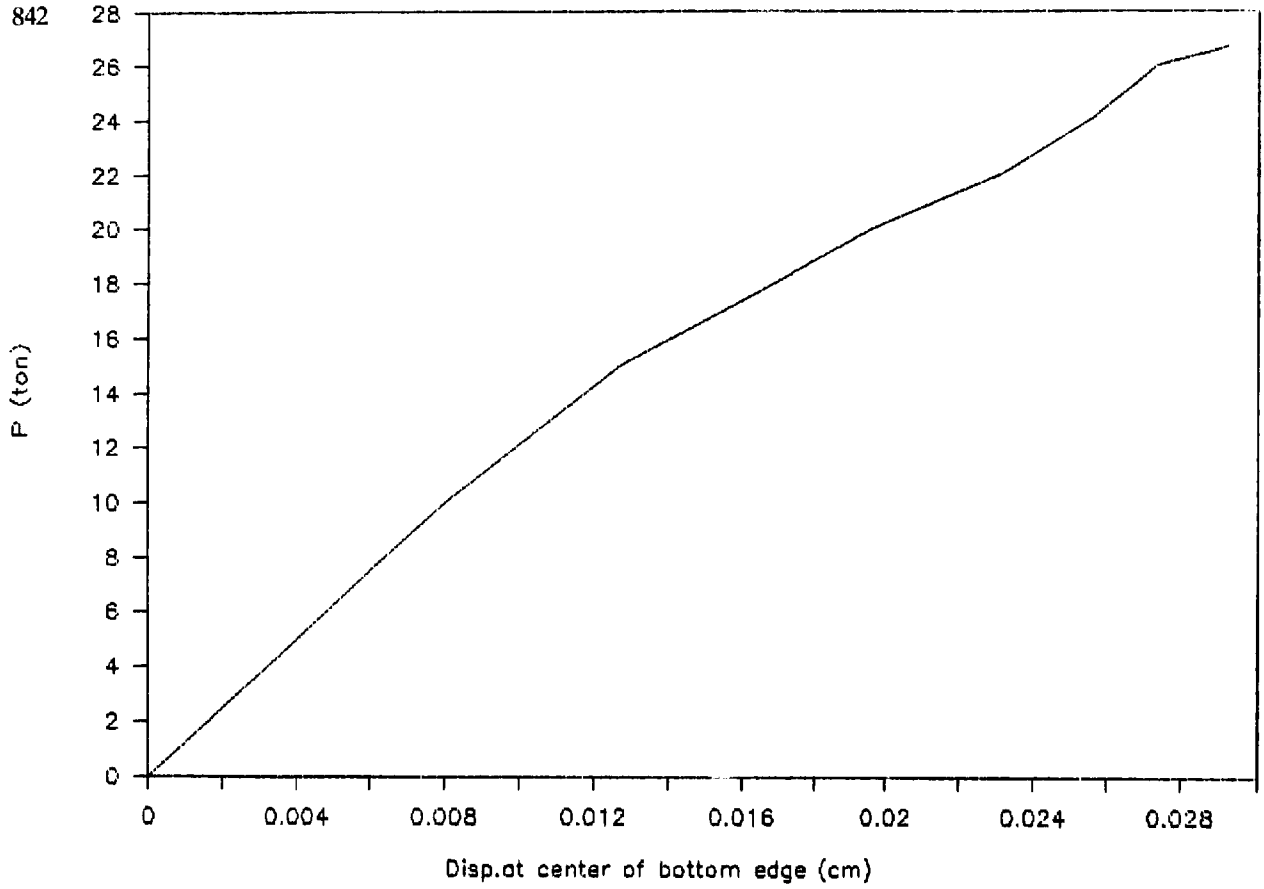

Fig. 8(b). Deep beam under two point loading. Load–displacement curve.

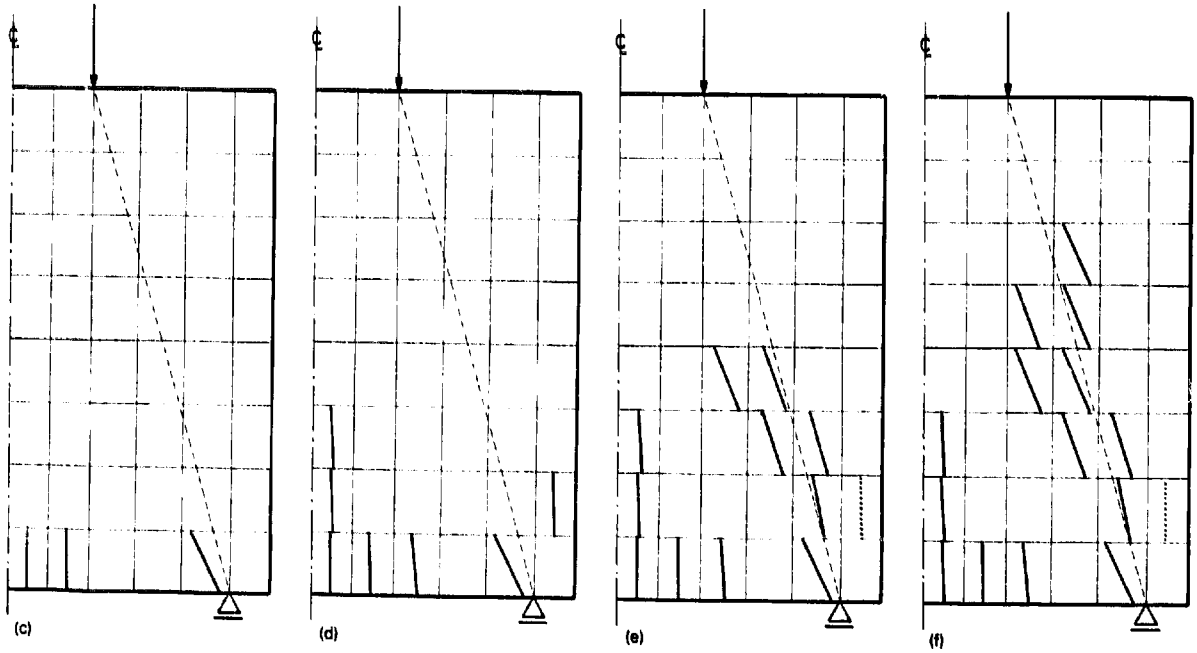

Fig. 8. Deep beam under two point loading. (c) Crack pattern for $P = 15$ ton; (d) crack pattern for $P = 20$ ton; (e) crack pattern for $P = 24$ ton (···· closed crack); (f) crack pattern for $P = 26$ ton (···· closed crack).

5. Conclusions

For a finite element formulation to be used as a reliable tool for engineering analysis the following requirements need to be satisfied:
- The formulation must not contain spurious zero-energy modes.
- The formulation must provide the 'exact solution' for constant stress problems which in the present context is equivalent to Irons' Patch Test.
- The formulation must be relatively insensitive to mesh distortions and changes in material properties.

In [1, 9] it was shown that the QMITC element satisfies the above requirements, while in [2] it was shown that the formulation of finite elements with displacement interpolated embedded localization lines also fulfils the reliability criteria and, in fracture problems, dissipates the correct energy.

In the present paper we use displacement interpolated localization lines embedded in QMITC elements to analyze the fracture propagation in some concrete structures.

The obtained results are very encouraging and allow us to consider the combined formulation (QMITC elements + displacement interpolated embedded localization lines) as an effective and reliable engineering tool.

Our next step will be to extend the present analysis procedure to the modelling of fracture propagation in metals and to the analysis of shear bands in metal forming processes.

References

[1] E.N. Dvorkin and S.I. Vassolo, A quadrilateral 2D finite element based on mixed interpolation of tensorial components, Engrg. Comput. 6 (1989) 217–224.
[2] E.N. Dvorkin, A.M. Cuitiño and G. Gioia, Finite elements with displacement interpolated embedded localization lines insensitive to mesh size and distortions, Internat. J. Numer. Methods Engrg. 30 (1990) 541–564.
[3] E.N. Dvorkin, A.M. Cuitiño and G. Gioia, A concrete material model based on non-associated plasticity and fracture, Engrg. Comput. 6 (1989) 281–294.
[4] E.N. Dvorkin and K.J. Bathe, A continuum mechanics based four-node shell element for general nonlinear analysis, Engrg. Comput. 1 (1984) 77–88.
[5] K.J. Bathe and E.N. Dvorkin, A four-node plate bending element based on Mindlin–Reissner plate theory and a mixed interpolation, Internat. J. Numer. Methods Engrg. 21 (1985) 367–385.
[6] K.J. Bathe and E.N. Dvorkin, A formulation of general shell elements – The use of mixed interpolation of tensorial components, Internat. J. Numer. Methods Engrg. 22 (1986) 697–722.
[7] K.J. Bathe, Finite Element Procedures in Engineering Analysis (Prentice-Hall, Englewood Cliffs, NJ, 1982).
[8] E.N. Dvorkin and M.E. Canga, Incompressible viscoplastic flow analysis using a quadrilateral 2D element based on mixed interpolation of tensorial components, submitted.
[9] E.N. Dvorkin and A.P. Assanelli, Elasto-plastic analysis using a quadrilateral 2D element based on mixed interpolation of tensorial components, in: D.R.J. Owen, E. Hinton and E. Oñate, eds., Proc. Second International Conference on Computational Plasticity (Pineridge, Swansea, UK, 1989).
[10] Z.P. Bažant, Instability, ductility and size effect in strain softening concrete, ASCE J. Engrg. Mech. 102 (1976) 331–344.
[11] A. Hillerborg, M. Modéer and P.E. Petersson, Analysis of crack formation and crack growth by means of fracture mechanics and finite elements, Cement Concr. Res. 6 (1976) 773–782.

[12] Z.P. Bažant and B.H. Oh, Crack band theory for fracture of concrete, RILEM, Mat. Struct. 16 (1983) 155–177.
[13] Z.P. Bažant and B.H. Oh, Rock fracture via strain-softening finite elements, ASCE J. Engrg. Mech. 110 (1984) 1015–1035.
[14] N.S. Ottosen, Thermodynamic consequences of strain softening in tension, ASCE J. Engrg. Mech. 112 (1986) 1152–1164.
[15] R. de Borst, Non-linear analysis of frictional materials, Doctoral Thesis, Delft University, Netherlands, 1986.
[16] G. Pijaudier-Cabot, Z.P. Bažant and M. Tabbara, Comparison of various models for strain softening, Engrg. Comput. 5 (1988) 141–150.
[17] Y.R. Rashid, Analysis of prestressed concrete pressure vessels, Nucl. Engrg. Des. 7 (1968) 334–355.
[18] St. Pietruszczak and Z. Mroz, Finite element analysis of deformation of strain softening materials, Internat. J. Numer. Methods Engrg. 17 (1981) 327–334.
[19] M. Ortiz, Y. Leroy and A. Needleman, A finite element method for localized failure analysis, Comput. Methods Appl. Mech. Engrg 61 (1987) 189–214.
[20] J. Oliver, A consistent characteristic length for smeared cracking models, Internat. J. Numer. Methods Engrg. 28 (1989) 461–474.
[21] K.J. Bathe and E.N. Dvorkin, On the automatic solution of nonlinear finite element equations, Comput. & Structures 17 (1983) 871–879.
[22] J.G. Rots, P. Nauta, G.M.A. Kusters and J. Blaauwendraad, Smeared crack approach and fracture localization in concrete, HERON 30 (1985) 1–48.
[23] R. de Borst and P. Nauta, Non-orthogonal cracks in smeared finite element modeling, Engrg. Comput. 2 (1985) 35–46.
[24] O.C. Zienkiewicz and R.L. Taylor, The Finite Element Method, Fourth Edition, Vol. 1 (McGraw-Hill, New York, 1989).
[25] P.E. Petersson, Crack growth and development of fracture zones in plain concrete and similar materials, Report TVBM-1006, Lund Institute of Technology, Sweden, 1981.
[26] V. Ramakrishnan and Y. Ananthanarayana, Ultimate shear strength of deep beams in shear, ACI J. (February 1968) 87–98.
[27] D.V. Phillips and O.C. Zienkiewicz, Finite element non-linear analysis of concrete structures, Proc. Instn. Civ. Engrgs., Part 2, 61 (1976) 59–88.